ACS APPLIED MATERIALS & INTERFACES

Research Article

www.acsami.org

Enhanced Thermoelectric Performance of Bar-Coated SWCNT/P3HT Thin Films

Woohwa Lee,[†,‡,§] Cheon Taek Hong,[†,§] O Hwan Kwon,[†] Youngjae Yoo,[†] Young Hun Kang,[†] Jun Young Lee,[‡] Song Yun Cho,*[,†] and Kwang-Suk Jang*[,†]

[†]Division of Advanced Materials, Korea Research Institute of Chemical Technology, Daejeon 305-600, Republic of Korea

[‡]Department of Chemical Engineering, Sungkyunkwan University, Suwon 440-746, Republic of Korea

ABSTRACT: The influence of processing conditions, such as ink concentration and coating method, on the thermoelectric properties of SWCNT/P3HT nanocomposite films was investigated systematically. Using simple wire-bar-coating, SWCNT/P3HT nanocomposite films with high thermoelectric performance could be obtained without additional P3HT doping. The wire-bar-coated SWCNT/P3HT nanocomposite films exhibited power factors of up to 105 μW m^{-1} K^{-2} at room temperature. The SWCNT bundles with diameters in the range of 6−23 nm formed an interconnected network in the wire-bar-coated nanocomposite films. Network formation in these nanocomposite films was expected to be strongly related to the development of electrical pathways due to inter-SWCNT bundle connections. This study suggests that the thermoelectric performance of SWCNT/P3HT nanocomposite films could be optimized by controlling their processing conditions and morphology.

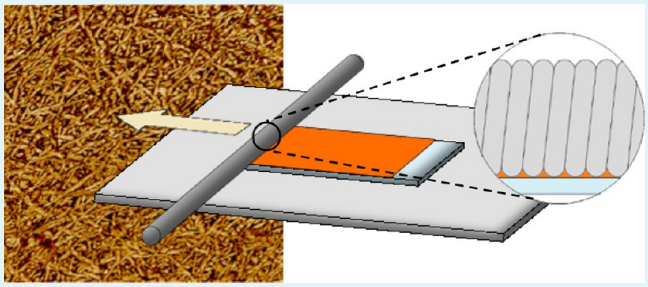

KEYWORDS: *thermoelectric, carbon nanotube, poly(3-hexylthiophene), nanocomposite, bar-coating, thin film*

INTRODUCTION

Thermoelectric materials are emerging green energy materials because they can convert waste heat into electricity via the Seebeck effect. The thermoelectric performance of materials can be evaluated by the dimensionless figure of merit, $ZT = S^2\sigma T/\kappa$, where S is the Seebeck coefficient, σ is the electrical conductivity, T is the absolute temperature, and κ is the thermal conductivity. Thermoelectric materials with a high Seebeck coefficient ($S = -\Delta V/\Delta T$, where ΔV is the thermoelectric voltage generated by a temperature difference of ΔT across a thermoelectric material), high electrical conductivity, and low thermal conductivity are expected to show good thermoelectric performance. Because direct measurement of the thermal conductivity of thin films is difficult, the power factor, $S^2\sigma$, is used as an alternative measure of thermoelectric performance.

Among the various types of thermoelectric materials, conjugated polymer-based materials are thought to be promising candidates for creating flexible low-cost printed thermoelectric generators.[1−11] However, the performance of conjugated polymer-based thermoelectric materials needs to be further improved to allow for their use in thermoelectric applications. In recent years, carbon nanotubes (CNTs) were found to be effective additives for enhancing the thermoelectric properties of conjugated polymers.[12−14] Yu et al. reported that single-walled CNT/poly(3,4-ethylenedioxythiophene)-poly(styrenesulfonate) (SWCNT/PEDOT−PSS) nanocomposite films exhibited power factors of up to 25 μW m^{-1} K^{-2} at room temperature.[12] Chen et al. reported that SWCNT/polyaniline nanocomposite films exhibited power factors of up to 176 μW m^{-1} K^{-2} at room temperature.[13] Poly(3-hexylthiophene) (P3HT) has also been considered for use as a conjugated polymer matrix. Because P3HT is soluble in common organic solvent, unlike many other conjugated polymers such as PEDOT, P3HT-based thermoelectric solutions or dispersions are suitable for various solution-processes including bar-coating, inkjet-printing, and screen-printing. Müller et al. reported that SWCNT/P3HT nanocomposite films doped with ferric chloride exhibited power factors of 95 ± 12 μW m^{-1} K^{-2} at room temperature.[14]

Even though CNT/conjugated polymer nanocomposite films exhibit excellent thermoelectric performance, there is a lack of research on the processing methods used in their preparation. It is well-known that the processing method has a direct impact on the morphology and physical properties of the resulting nanocomposite films. Because previously reported CNT/conjugated polymer nanocomposite films were mainly prepared by drop-casting, their morphologies and thermoelectric properties were not fully optimized.

In this study, we report a wire-bar-coating process for creating thermoelectric SWCNT/P3HT nanocomposite films in which SWCNTs form well-dispersed networks. These wire-bar-coated SWCNT/P3HT nanocomposite films exhibited excellent thermoelectric performance with power factors of up to 105 μW m^{-1} K^{-2} at room temperature. Interestingly, in

Received: December 2, 2014
Accepted: March 11, 2015
Published: March 11, 2015

DOI: 10.1021/acsami.5b00626
ACS Appl. Mater. Interfaces 2015, 7, 6550−6556

our process, P3HT doping is not necessary for obtaining high thermoelectric performance. Whereas, drop-cast SWCNT/undoped P3HT nanocomposite films have been reported to exhibit a power factor of only ~10 μW m^{-1} K^{-2} at room temperature.[14] For direct comparison, we also prepared drop-cast SWCNT/P3HT nanocomposite films; these films exhibited noticeably poorer thermoelectric performance. To the best of our knowledge, optimization of the thermoelectric performance of CNT/conjugated polymer nanocomposites by controlling processing conditions such as ink concentration and coating method has not yet been reported. Our results suggest that the processing method and morphology should be carefully considered for the enhancement of the thermoelectric properties of thermoelectric nanocomposites.

EXPERIMENTAL SECTION

Purified SWCNTs were purchased from Unidym. Regioregular P3HT (M_w 37 685 g mol^{-1}, regioregularity 98.5%) was purchased from Sigma-Aldrich. *o*-Dichlorobenzene (*o*DCB) was purchased from Junsei. All chemicals in this study were used as received. The P3HT was dissolved in *o*DCB. The SWCNTs were then added to this solution. The mixture was sonicated in an ice bath using a probe sonicator (VCX-750 Vibra-Cell, Sonics & Materials) at 10 W for 1 h. This ink was then bar-coated onto a glass substrate (76 mm × 52 mm). More precisely, a 6.35 mm diameter bar closely wound with a 32 μm diameter wire was used and the carrying speed of the wire-bar was maintained at 10 mm/s during the bar-coating process.

The Seebeck coefficients of the films were measured under dark ambient conditions utilizing a custom built system. Before measurement, silver paste was printed onto the SWCNT/P3HT nanocomposite films through a screen mask. Two silver electrodes, 5 mm in width, were separated by a distance of 20 mm. The temperature gradient between the two electrodes was varied from 1 to 15 °C. The thermoelectric voltage generated by the temperature difference was measured with a Keithley 2182A Nanovoltmeter. The electrical conductivity was measured by a four-probe method (Keithley 195A digital multimeter and Keithley 220 programmable current source). UV−vis spectra were recorded with a Scinco UV S-2100. The thickness of the SWCNT/P3HT nanocomposite films was determined with an alpha-step surface profiler (α-step DC50, KLA Tencor). The surface morphology of the SWCNT/P3HT nanocomposite films was observed with a field-emission scanning electron microscope (SEM, MIRA3, TESCAN) operating at 20 kV and a tapping-mode atomic force microscope (AFM, Nanoscope IV, Digital Instruments). The fracture surface morphology of the SWCNT/P3HT nanocomposite film was observed with a field-emission high-resolution SEM (HR-SEM, Magellan 400, FEI) operating at 3 kV. Thermal conductivity was calculated from the measured thermal diffusivity, density, and specific heat capacity. The thermal diffusivities of the films were determined by the laser flash method (ASTM E1461) with a Netzsch laser flash thermal diffusivity apparatus (LFA 447 NanoFlash). The density and specific heat capacity of the films were measured with a Protech Gas Pycnometer (Accupyc 1330) and a TA Instruments modulated differential scanning calorimeter (MDSC Q200), respectively.

RESULTS AND DISCUSSION

Because *o*DCB is a good solvent for P3HT, the strong $\pi-\pi$ interaction between P3HT and SWCNT is advantageous for SWCNT dispersion in the ink. To investigate the effect of the SWCNT composition on the thermoelectric properties of the nanocomposite films, the composition was varied while keeping the total solid concentration of the inks fixed at 2 mg mL^{-1}. After sonication of the mixture, the inks were stable for more than 1 day without any precipitation. We investigated the interaction between P3HT and SWCNT by UV−vis spectra. Figure 1 shows the UV−vis spectra of the SWCNT dispersion

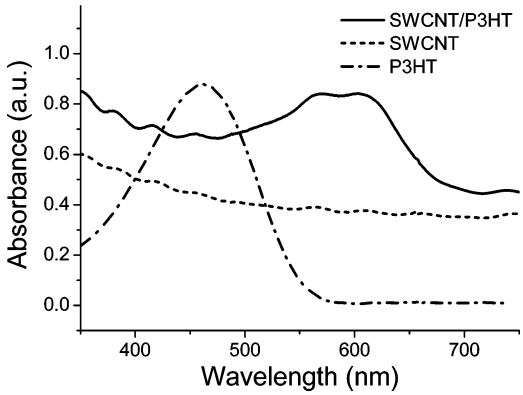

Figure 1. UV−vis spectra of the SWCNT dispersion in *o*DCB, P3HT solution in *o*DCB, and SWCNT/P3HT ink with 60 wt % SWCNTs.

in *o*DCB, P3HT solution in *o*DCB, and SWCNT/P3HT ink with 60 wt % SWCNTs. The SWCNT dispersion showed no characteristic peaks. The P3HT solution exhibited an absorption peak centered at 460 nm, which is a characteristic peak of the regioregular P3HT with a rod-like chain conformation.[15,16] Interestingly, a red shift of absorption was observed in the SWCNT/P3HT ink. The absorption peaks centered at 568 and 604 nm coincide with peaks from solid state regioregular P3HT, characteristic peaks of $\pi-\pi$ stacked P3HT chains.[15−17] The red shift in this study indicates $\pi-\pi$ interaction between P3HT and SWCNT in the ink. The $\pi-\pi$ interaction between P3HT and SWCNT might be the main reason for the dispersion stability of the SWCNT/P3HT ink. Using a simple wire-bar-coating process, SWCNT/P3HT nanocomposite films were prepared (Figure 2). The volume

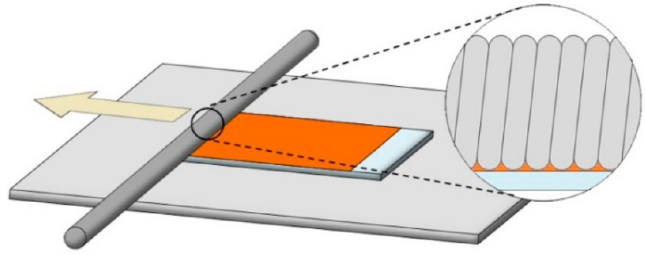

Figure 2. Schematic diagram of the wire-bar-coating process.

of the gap between the substrate and wire-bar was precisely determined by varying the diameters of the bar and wire wound closely onto the bar surface. When using inks with less than 20 wt % SWCNT, films were not formed by the wire-bar-coating due to the low viscosity. The nanocomposite films prepared from inks with more than 70 wt % SWCNT were not uniform. However, uniform SWCNT/P3HT nanocomposite films were prepared from inks with 30, 40, 50, and 60 wt % SWCNT. A dependence of the film thickness, measured to be in the range of 41−53 nm, on the quantity of SWCNT present in the ink was not found.

To estimate the thermoelectric properties of the SWCNT/P3HT nanocomposite films as a function of SWCNT composition, the SWCNT composition-dependent Seebeck coefficient, electrical conductivity, and power factor were measured, as shown in Figure 3. The SWCNT composition significantly affects the thermoelectric properties of the SWCNT/P3HT nanocomposite films. As the SWCNT

DOI: 10.1021/acsami.5b00626
ACS Appl. Mater. Interfaces 2015, 7, 6550−6556

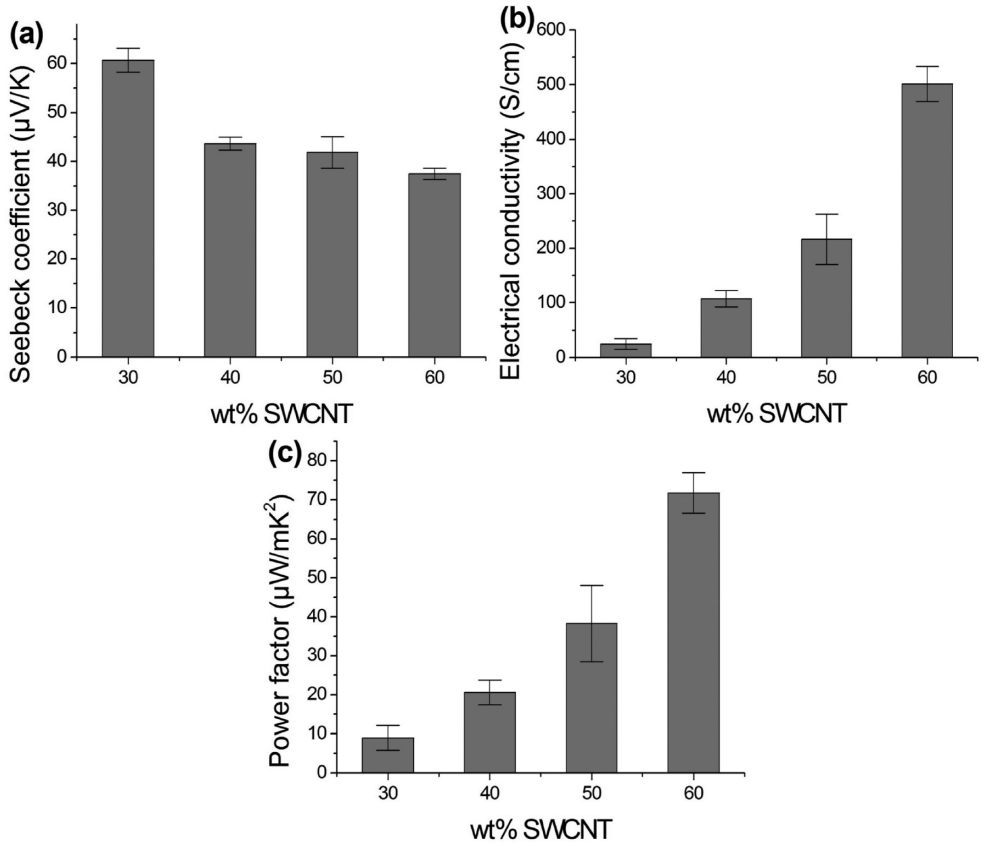

Figure 3. Dependence of the (a) Seebeck coefficient, (b) electrical conductivity, and (c) power factor on the quantity of SWCNTs in the SWCNT/P3HT nanocomposite films.

composition increased, the Seebeck coefficient decreased and the electrical conductivity drastically increased. The Seebeck coefficient and electrical conductivity of the nanocomposite film with 30 wt % SWCNT were 60.7 ± 2.4 μV K^{-1} and 24.8 ± 9.9 S cm^{-1}, and those with 60 wt % SWCNT were 37.5 ± 1.1 μV K^{-1} and 501 ± 32 S cm^{-1}, respectively. The power factor, calculated from the measured Seebeck coefficient and electrical conductivity, increased as the SWCNT composition increased. The power factors of nanocomposite films prepared with 30 and 60 wt % SWCNTs 8.99 ± 3.16 μW m^{-1} K^{-2} and 71.8 ± 5.2 μW m^{-1} K^{-2}, respectively. This increase in the power factor originated from the drastic increase in the electrical conductivity of the films. As the SWCNT composition increased, the density of the SWCNT−SWCNT junctions in the wire-bar-coated nanocomposite films was expected to increase exponentially.

Figure 4 shows the SEM images of the wire-bar-coated SWCNT/P3HT nanocomposite films. The SWCNTs composition significantly affects the surface morphology of the films. As the SWCNT composition increased, the network of SWCNT bundles in the nanocomposite films was more clearly visible. Network formation in the nanocomposite film should be related to the electrical pathways composed of inter-SWCNT bundle connections. Figure 5 shows the AFM images of the wire-bar-coated SWCNT/P3HT nanocomposite film with 60 wt % SWCNTs. An interconnected network of one-dimensional SWCNT bundles with diameters in the range of 6−23 nm was observed in the AFM height and phase images. From the surface morphologies of the films, it can be concluded that SWCNTs were well-dispersed in the ink and that the

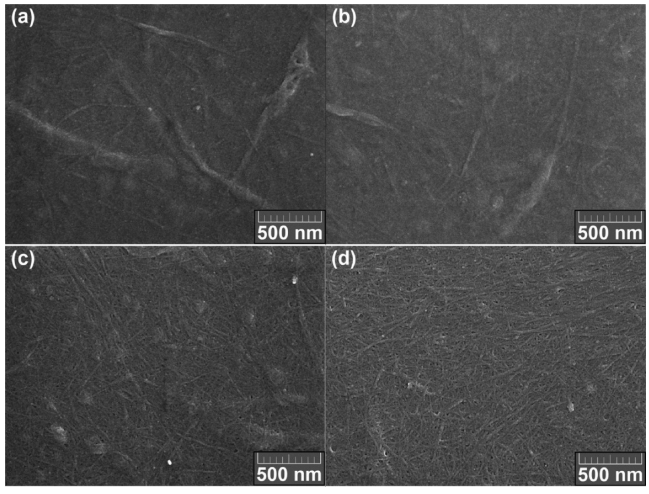

Figure 4. SEM images of the wire-bar-coated SWCNT/P3HT nanocomposite films with (a) 30, (b) 40, (c) 50, and (d) 60 wt % SWCNTs.

strong $\pi-\pi$ interaction between P3HT and SWCNT efficiently prevented restacking of the SWCNTs.

The wire-bar-coated film thickness and quality have been observed to be significantly affected by the total solid content of the ink, wire diameter, and carrying speed of the wire-bar.[18−20] To investigate the effect of ink concentration on the thermoelectric properties of the films, we varied only the total solid content of the ink while all other parameters such as wire diameter and carrying speed of the wire-bar were kept

DOI: 10.1021/acsami.5b00626
ACS Appl. Mater. Interfaces 2015, 7, 6550−6556

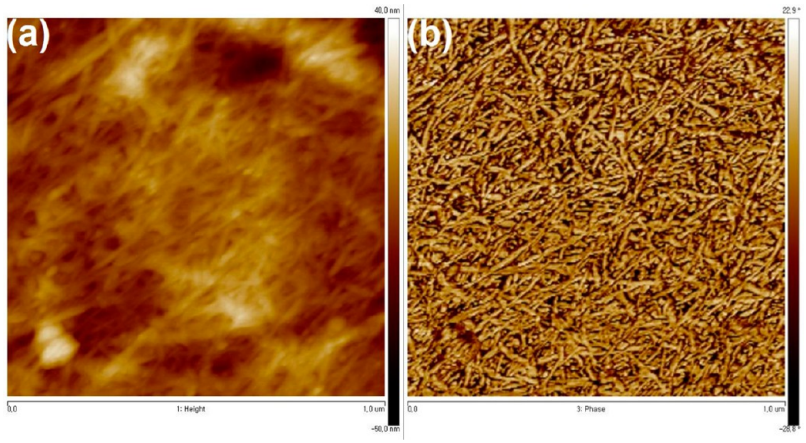

Figure 5. AFM (a) height and (b) phase images (1 μm × 1 μm) of the wire-bar-coated SWCNT/P3HT nanocomposite film with 60 wt % SWCNTs.

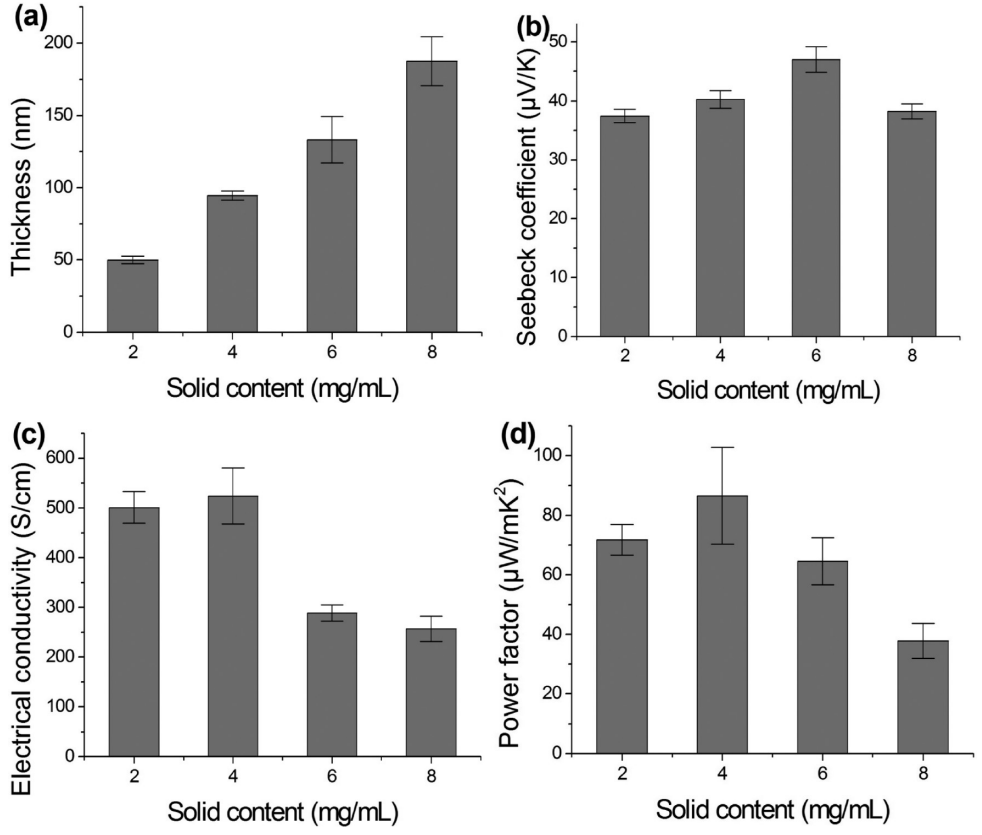

Figure 6. Solid content dependence of the (a) thickness, (b) Seebeck coefficient, (c) electrical conductivity, and (d) power factor of the SWCNT/P3HT nanocomposite films.

constant. The SWCNT composition was also fixed at 60 wt %. Figure 6 shows the variations in thickness, Seebeck coefficient, electrical conductivity, and power factor of the SWCNT/P3HT nanocomposite films as a function of the total solid concentration of the ink. The thickness of the wire-bar-coated films was controlled and found to be in the range of 50 to 188 nm. The Seebeck coefficient slightly increased with increasing total solid content, reaching a peak of 47.0 ± 2.2 μV K^{-1} for the film prepared with the 6 mg mL^{-1} ink. The electrical conductivity of the films from the 6 mg mL^{-1} and 8 mg mL^{-1} inks, 289 ± 17 S cm^{-1} and 257 ± 26 S cm^{-1}, are much lower than those with the 2 mg mL^{-1} and 4 mg mL^{-1} inks, 501 ± 32 S cm^{-1} and 524 ± 56 S cm^{-1}, respectively. The electrical properties of CNT/polymer nanocomposites have been observed to be strongly affected by the dispersion state of CNTs.[21−24] The degree of dispersion of the 1-dimensional CNT bundles is positively related to the density of the CNT-CNT junctions. The SWCNTs, in this study, might, therefore, be better dispersed in the less concentrated inks. The maximum power factor was calculated to be 105 μW m^{-1}K^{-2} for an ink with a total solid content of 4 mg mL^{-1}. Interestingly, to achieve the high thermoelectric performance observed here, additional P3HT doping is not necessary. It is noteworthy that drop-cast SWCNT/undoped P3HT nanocomposite films have

DOI: 10.1021/acsami.5b00626
ACS Appl. Mater. Interfaces 2015, 7, 6550−6556

been observed to exhibit power factors of only ~10 μW m^{-1} K^{-2}.[14] After submersion in a $FeCl_3$/nitromethane solution for P3HT doping, these drop-cast nanocomposite films exhibited power factors of 95 ± 12 μW m^{-1} K^{-2}.[14] The thermoelectric performance of the wire-bar-coated SWCNT/undoped P3HT nanocomposite films, in this study, is comparable to that of the drop-cast SWCNT/P3HT doped with $FeCl_3$, as summarized in Table 1. Elimination of the doping process would be advantageous for thermoelectric applications because of improved processability.

Table 1. Summary of the Thermoelectric Properties of the SWCNT/P3HT Nanocomposite Films with Comparison to Previously Reported Data

coating method	dopant	power factor (μW m^{-1}K^{-2})	ref
drop-casting	$FeCl_3$	95 ± 12	14
drop-casting	none	~10	14
drop-casting	none	41.7 ± 12.5	this work
wire-bar-coating	none	86.6 ± 16.2	this work

For comparison, we also prepared drop-cast SWCNT/P3HT nanocomposite films using the 4 mg mL^{-1} ink with 60 wt % SWCNTs. Depending on the coating method, the film thickness was significantly different. The thicknesses of the wire-bar-coated and drop-cast films were 94.6 ± 3.2 nm and 7.37 ± 0.94 μm, respectively. The Seebeck coefficient, electrical conductivity, and power factor of the wire-bar-coated films were 40.3 ± 1.5 μV K^{-1}, 524 ± 56 S cm^{-1}, and 86.6 ± 16.2 μW m^{-1} K^{-2}, whereas those of the drop-cast films were 32.7 ± 3.8 μV K^{-1}, 383 ± 47 S cm^{-1}, and 41.7 ± 12.5 μW m^{-1} K^{-2}, respectively. The wire-bar-coated SWCNT/P3HT nanocomposite films showed noticeably better thermoelectric performance, as summarized in Table 1. Figure 7 shows the SEM

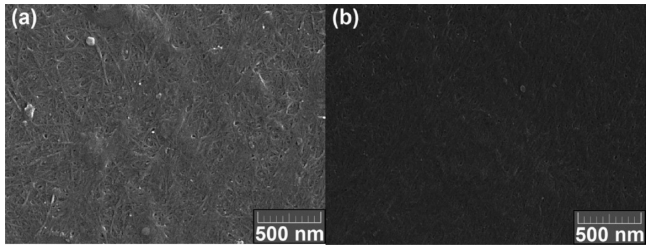

Figure 7. SEM images of the (a) wire-bar-coated and (b) drop-cast SWCNT/P3HT nanocomposite films prepared using the 4 mg mL^{-1} ink with 60 wt % SWCNTs.

images of the wire-bar-coated and drop-cast SWCNT/P3HT nanocomposite films prepared using the 4 mg mL^{-1} ink with 60 wt % SWCNT. An interconnected network of SWCNT bundles is clearly visible in the wire-bar-coated film. However, in the case of the drop-cast film, a rather smooth surface is observed. Figure 8 shows the AFM height and phase images of the same wire-bar-coated and drop-cast SWCNT/P3HT nanocomposite films. An interconnected network of 1-dimensional SWCNT bundles with diameters in the range of 6−28 nm is clearly visible in the AFM images of the wire-bar-coated film. On the other hand, the drop-cast film shows much thicker bundles with diameters in the range of 28−56 nm and a largely reduced interconnection density. The dispersion state of SWCNTs in the ink could be directly transferred onto the wire-bar-coated film because of the fast film formation by the high carrying speed of the wire-bar of 10 mm/s. However, in the case of drop-casting, a few hours are needed for solvent drying. During solvent evaporation, the ink would become more concentrated and the dispersion state of the SWCNTs could change. In this concentrated ink, the SWCNT bundles could form some agglomerates, which could reduce the density of the SWCNT−SWCNT junctions in the final nanocomposite films. To confirm the inter-SWCNT bundle connections, HR-SEM image of the fracture surface of the wire-bar-coated SWCNT/P3HT nanocomposite film was obtained (Figure 9). The SWCNT bundles that might be wrapped by P3HT chains are densely interconnected.

To estimate the thermoelectric properties, we require information about the thermal conductivity ($\kappa = C_p\rho\alpha$, where C_p, ρ, and α are specific heat capacity, density, and thermal diffusivity, respectively). Unfortunately, because of our experimental limitations, thermal conductivities of the wire-bar-coated thin films were not directly measured. Instead, the specific heat capacities, densities, and thermal diffusivities of 38 μm thick P3HT and 11 μm thick SWCNT/P3HT nanocomposite freestanding films were measured. The thermal conductivity of the P3HT films was calculated to be 0.18 ± 0.02 W m^{-1} K^{-1}, which agrees well with previously reported values.[10,14] Surprisingly, despite a high SWCNT composition (60 wt %), the thermal conductivity of the SWCNT/P3HT nanocomposite films, 0.085 ± 0.006 W m^{-1} K^{-1}, was much lower than that of the P3HT films. This reduced thermal conductivity might be due to the blockage of phonon transport through the nanostructured interfaces, which can function as a scattering sites of phonons.[14,25−28] Similar behaviors in SWCNT/P3HT, SWCNT/PEDOT−PSS, SWCNT/polyaninile, and Te/PEDOT−PSS nanocomposite films have been reported.[14,25−28] The addition of SWCNTs could enhance the electrical conductivity of the nanocomposite films, however, the increase in the thermal conductivity might be impeded by phonon scattering. Note that the in-plane thermal conductivity of the wire-bar-coated SWCNT/P3HT nanocomposite films might be higher than the through-plane thermal conductivity of the freestanding films. Generally, thermal conductivity, κ, of thermoelectric materials can be expressed as a sum of the electronic thermal conductivity, κ_e, and the lattice thermal conductivity, κ_l ($\kappa = \kappa_e + \kappa_l$). The electronic thermal conductivity can be calculated by Weidemann-Franz relation, $\kappa_e = L_0\sigma T$, where L_0 is Lorentz constant of 2.45 × 10^{-8} V^2 K^{-2}, σ is the electrical conductivity, and T is the absolute temperature. From the in-plane electrical conductivity of 524 S cm^{-1}, the electronic thermal conductivity of the wire-bar-coated SWCNT/P3HT nanocomposite film is calculated to be 0.38 W m^{-1} K^{-1}, which is higher than the thermal conductivity of the SWCNT/P3HT nanocomposite freestanding films.

We demonstrated that the wire-bar-coated SWCNT/P3HT nanocomposite films exhibited excellent thermoelectric performance. The thermoelectric properties of the wire-bar-coated SWCNT/P3HT nanocomposite films were optimized by controlling the SWCNT composition and total solid content of the ink. The thermoelectric performance could be discussed with the density of the nanocomposite films, as well as the interconnection density of the SWCNT bundles. For example, as the total void volume of the film increases, the electrical conductivity should decrease. Formation of the nanoscopic voids in the nanocomposite films might be influenced by the processing method. The research work to investigate the effect of the film density on the thermoelectric performance and the

DOI: 10.1021/acsami.5b00626
ACS Appl. Mater. Interfaces 2015, 7, 6550−6556

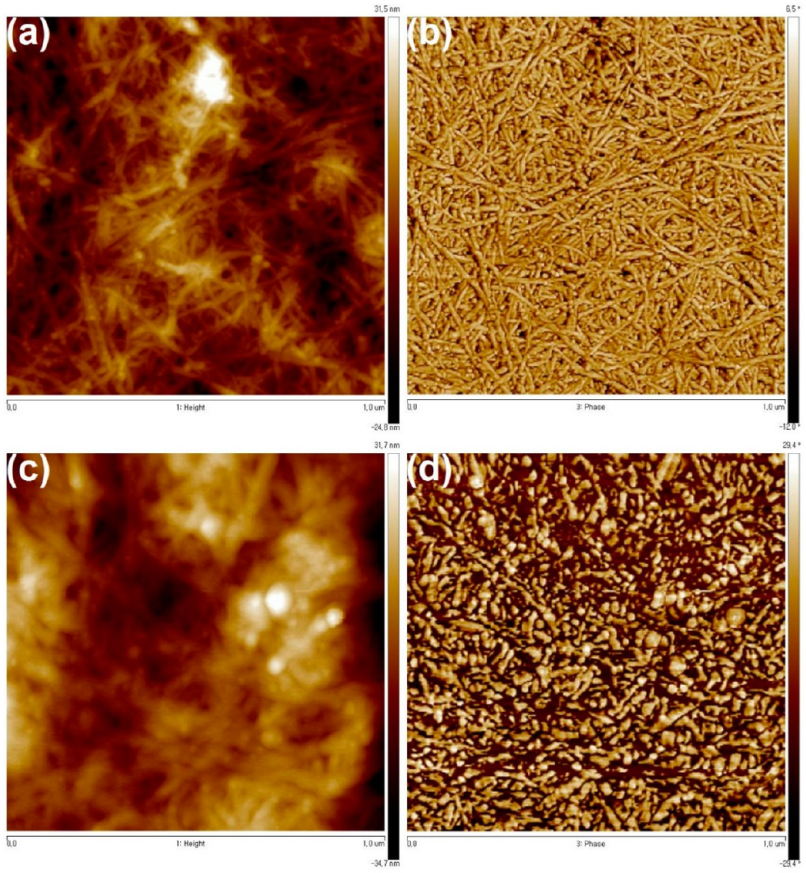

Figure 8. AFM height and phase images (1 μm × 1 μm) of the (a, b) wire-bar-coated and (c, d) drop-cast SWCNT/P3HT nanocomposite films, prepared using the 4 mg mL^{-1} ink with 60 wt % SWCNTs.

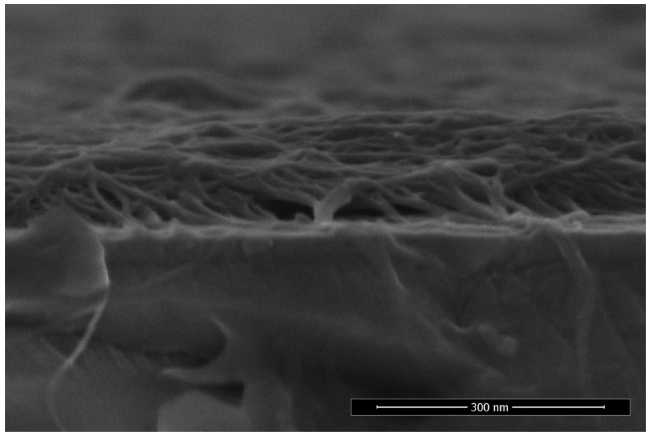

Figure 9. HR-SEM image of the fracture surface of the wire-bar-coated SWCNT/P3HT nanocomposite film prepared using the 4 mg mL^{-1} ink with 60 wt % SWCNTs.

densification methods of the nanocomposite films such as hot rolling is currently being investigated.

CONCLUSION

Using a wire-bar-coating process, we prepared SWCNT/P3HT nanocomposite films in which SWCNT bundles with diameters in the range of 6−23 nm developed an interconnected network. The wire-bar-coated SWCNT/P3HT nanocomposite films exhibited excellent thermoelectric properties with power factors of up to 105 μW m^{-1}K^{-2} at room temperature. Such a high thermoelectric performance did not require additional P3HT doping. To investigate the effect of the coating method on the thermoelectric properties of the film, drop-cast SWCNT/P3HT nanocomposite films were prepared and their thermoelectric properties compared with those of the wire-bar-coated films. The drop-cast films exhibited noticeably poorer thermoelectric performance. We found that processing conditions such as ink concentration and coating method significantly affected the surface morphology and thermoelectric properties of the SWCNT/P3HT nanocomposite films, and should be carefully considered for the enhancement of their thermoelectric performance.

AUTHOR INFORMATION

Corresponding Authors

*E-mail kjang@krict.re.kr.
*E-mail scho@krict.re.kr

Author Contributions

§W.L. and C.T.H. contributed equally to this work.

Notes

The authors declare no competing financial interest.

ACKNOWLEDGMENTS

This work was supported by a grant from the KRICT Core Project (KK-1407-B6), a grant from the R&D Convergence Program funded by the National Research Council of Science & Technology, and the Center for Advanced Soft-Electronics funded by the Ministry of Science, ICT and Future Planning as Global Frontier Project (2011-0031628).

DOI: 10.1021/acsami.5b00626
ACS Appl. Mater. Interfaces 2015, 7, 6550−6556

REFERENCES

(1) He, M.; Qiu, F.; Lin, Z. Toward High-Performance Polymer-Based Thermoelectric Materials. *Energy Environ. Sci.* **2013**, *6*, 1352−1361.

(2) Chabinyc, M. Thermoelectric Polymers: Behind Organics' Thermopower. *Nat. Mater.* **2014**, *13*, 119−121.

(3) Sun, Y.; Sheng, P.; Di, C.; Jiao, F.; Xu, W.; Qiu, D.; Zhu, D. Organic Thermoelectric Materials and Devices Based on *p*- and *n*-type Poly(Metal 1,1,2,2-Ethenetetrathiolate)s. *Adv. Mater.* **2012**, *24*, 932−937.

(4) Bubnova, O.; Khan, Z. U.; Malti, A.; Braun, S.; Fahlman, M.; Berggren, M.; Cripsin, X. Optimization of the Thermoelectric Figure of Merit in the Conducting Polymer Poly(3,4-Ethylenedioxythiophene). *Nat. Mater.* **2011**, *10*, 429−433.

(5) Kim, G.-H.; Shao, L.; Zhang, K.; Pipe, K. P. Engineered Doping of Organic Semiconductors for Enhanced Thermoelectric Efficiency. *Nat. Mater.* **2013**, *12*, 719−723.

(6) Park, T.; Park, C.; Kim, B.; Shin, H.; Kim, E. Flexible PEDOT Electrodes with Large Thermoelectric Power Factors to Generate Electricity by the Touch of Fingertips. *Energy Environ. Sci.* **2013**, *6*, 788−792.

(7) Lee, S. H.; Park, H.; Kim, S.; Son, W.; Cheong, I. W.; Kim, J. H. Transparent and Flexible Organic Semiconductor Nanofilms with Enhanced Thermoelectric Efficiency. *J. Mater. Chem. A* **2014**, *2*, 7288−7294.

(8) Culebras, M.; Gómez, C. M.; Cantarero, A. Enhanced Thermoelectric Performance of PEDOT with Different Counter-Ions Optimized by Chemical Reduction. *J. Mater. Chem. A* **2014**, *2*, 10109−10115.

(9) Zhang, Q.; Sun, Y.; Xu, W.; Zhu, D. Thermoelectric Energy from Flexible P3HT Films Doped with a Ferric Salt of Triflimide Anions. *Energy Environ. Sci.* **2012**, *5*, 9639−9644.

(10) He, M.; Ge, J.; Lin, Z.; Feng, X.; Wang, X.; Lu, H.; Yang, Y.; Qiu, F. Thermopower Enhancement in Conducting Polymer Nanocomposites via Carrier Energy Scattering at Organic/Inorganic Semiconductor Interface. *Energy Environ. Sci.* **2012**, *5*, 8351−8358.

(11) Shi, H.; Liu, C.; Xu, J.; Song, H.; Lu, B.; Jiang, F.; Zhou, W.; Zhang, G.; Jiang, Q. Facile Fabrication of PEDOT:PSS/Polythiophenes Bilayered Nanofilms on Pure Organic Electrodes and Their Thermoelectric Performance. *ACS Appl. Mater. Interfaces* **2013**, *5*, 12811−12819.

(12) Kim, D.; Kim, Y.; Choi, K.; Grunlan, J. C.; Yu, C. Improved Thermoelectric Behavior of Nanotube-Filled Polymer Composites with Poly(3,4-Ethylenedioxythiophene) Poly(Styrenesulfonate). *ACS Nano* **2010**, *4*, 513−523.

(13) Yao, Q.; Wang, Q.; Wang, L.; Chen, L. Abnormally Enhanced Thermoelectric Transport Properties of SWNT/PANI Hybrid Films by the Strengthened PANI Molecular Ordering. *Energy Environ. Sci.* **2014**, *7*, 3801−3807.

(14) Bounioux, C.; Díaz-Chao, P.; Campoy-Quiles, M.; Martín-González, M. S.; Goñi, A. R.; Yerushalmi-Rozen, R.; Müller, C. Thermoelectric Composites of Poly(3-Hexylthiophene) and Carbon Nanotubes with a Large Power Factor. *Energy Environ. Sci.* **2013**, *6*, 918−925.

(15) Chen, T.-A.; Wu, X.; Rieke, R. D. Regiocontrolled Synthesis of Poly(3-Alkylthiophenes) Mediated by Rieke Zinc: Their Characterization and Solid-State Properties. *J. Am. Chem. Soc.* **1995**, *117*, 233−244.

(16) Zou, J.; Liu, L.; Chen, H.; Khondaker, S. I.; McCullough, R. D.; Huo, Q.; Zhai, L. Dispersion of Pristine Carbon Nanotubes Using Conjugated Block Copolymers. *Adv. Mater.* **2008**, *20*, 2055−2060.

(17) Ai, X.; Anderson, N.; Guo, J.; Kowalik, J.; Tolbert, L. M.; Lian, T. Ultrafast Photoinduced Charge Separation Dynamics in Polythiophene/SnO_2 Nanocomposites. *J. Phys. Chem. B* **2006**, *110*, 25496−25503.

(18) Ouyang, J.; Guo, T.-F.; Yang, Y.; Higuchi, H.; Yoshioka, M.; Nagatsuka, T. High-Performance, Flexible Polymer Light-Emitting Diodes Fabricated by a Continuous Polymer Coating Process. *Adv. Mater.* **2002**, *14*, 915−918.

(19) Khim, D.; Han, H.; Baeg, K.-J.; Kim, J.; Kwak, S. W.; Kim, D.-Y.; Noh, Y. Y. Simple Bar-Coating Process for Large-Area, High-Performance Organic Field-Effect Transistors and Ambipolar Complementary Integrated Circuits. *Adv. Mater.* **2013**, *25*, 4302−4308.

(20) Tracton, A. A. *Coatings Technology Handbook*, 3rd ed.; CRC Press: Boca Raton, FL, 2006.

(21) Song, Y. S.; Youn, J. R. Influence of Dispersion States of Carbon Nanotubes on Physical Properties of Epoxy Nanocomposites. *Carbon* **2005**, *43*, 1378−1385.

(22) Li, J.; Ma, P. C.; Chow, W. S.; To, C. K.; Tang, B. Z.; Kim, J.-K. Correlations between Percolation Threshold, Dispersion State, and Aspect Ratio of Carbon Nanotubes. *Adv. Funct. Mater.* **2007**, *17*, 3207−3215.

(23) Chang, T.-E.; Kisliuk, A.; Rhodes, S. M.; Brittain, W. J.; Sokolov, A. P. Conductivity and Mechanical Properties of Well-Dispersed Single-Wall Carbon Nanotube/Polystyrene Composite. *Polymer* **2006**, *47*, 7740−7746.

(24) Kim, Y. J.; Shin, T. S.; Choi, H. D.; Kwon, J. H.; Chung, Y.-C.; Yoon, H. G. Electrically Conductivity of Chemically Modified Multiwalled Carbon Nanotube/Epoxy Composites. *Carbon* **2005**, *43*, 23−30.

(25) Kim, Y. J.; Shin, T. S.; Choi, H. D.; Kwon, J. H.; Chung, Y.-C.; Yoon, H. G. Electrically Conductivity of Chemically Modified Multiwalled Carbon Nanotube/Epoxy Composites. *Carbon* **2005**, *43*, 23−30.

(26) Yu, C.; Choi, K.; Yin, L.; Grunlan, J. C. Light-Weight Flexible Carbon Nanotube Based Organic Composites with Large Thermoelectric Power Factors. *ACS Nano* **2011**, *5*, 7885−7892.

(27) Yu, C.; Choi, K.; Yin, L.; Grunlan, J. C. Enhanced Thermoelectric Performance of Single-Walled Carbon Nanotubes/Polyaniline Hybrid Nanocomposites. *ACS Nano* **2010**, *4*, 2445−2451.

(28) See, K. C.; Feser, J. P.; Chen, C. E.; Majumdar, A.; Urban, J. J.; Segalman, R. A. Water-Processsable Polymer-Nanocrystal Hybrids for Thermoelectrics. *Nano Lett.* **2010**, *10*, 4664−4667.

DOI: 10.1021/acsami.5b00626
ACS Appl. Mater. Interfaces 2015, 7, 6550−6556